Petroleum Science 23 (2026) 4243–4258

Contents lists available at ScienceDirect

Petroleum Science

journal homepage: www.keaipublishing.com/en/journals/petroleum-science

Original Paper

A resilience-oriented transient optimization approach for emergency operation of natural gas pipeline systems with linepack dynamics and priority-based load shedding

Si-Rui Zhao [a], Li-Li Zuo [a,*], Feng Zhu [b], Bing-Lang He [a], Chang-Chun Wu [a,**]

[a] National Engineering Laboratory for Pipeline Safety/Beijing Key Laboratory of Urban Oil and Gas Distribution Technology, China University of Petroleum (Beijing), Beijing, 102249, China
[b] PetroChina Planning & Engineering Institute, Beijing, 100083, China

A R T I C L E I N F O

Article history:
Received 11 February 2026
Received in revised form
27 April 2026
Accepted 26 May 2026
Available online 2 June 2026

Edited by Meng-Jiao Zhou

Keywords:
Resilience-oriented emergency operation
Linepack dynamics
Transient hydraulics
Priority-based load shedding
Natural gas pipeline system

A B S T R A C T

Under extreme disturbances, the safety of natural gas pipeline networks is governed by transient capabilities to sustain fuel delivery rather than steady-state balance. Existing studies, often grounded in static assumptions, fail to capture the nonlinear coupling among linepack dynamics, operational regulation, and demand response. To address this limitation, this study proposes a resilience-oriented optimization approach that integrates transient hydraulics with priority-based load shedding. From an operational perspective, system response to extreme disturbances can be interpreted through a hierarchical defense mechanism comprising passive buffering, active regulation, and adaptive degradation. Two metrics, system survival time and resilience limit, are introduced to quantify the operational boundaries of emergency conditions. A nonlinear programming model is developed by explicitly coupling transient flow equations, compressor constraints, and time-dependent response delays. Case studies on supply interruption and demand surge scenarios reveal distinct mechanisms governing system resilience. In supply interruption scenarios, resilience relies on the synergy between linepack buffering and intervention timing; notably, decision latency is found to nonlinearly amplify the required load shedding intensity. Explicitly utilizing this temporal buffer can reduce required load shedding by approximately 74% compared to steady-state models. Conversely, under demand surge scenarios, system failure is dictated by topological transmission bottlenecks (identified at a 32% demand surge limit), indicating that operational regulation alone cannot break through the inherent resilience ceiling. Furthermore, effective load shedding strategies must account for the spatial hydraulic effectiveness of demand nodes. These findings provide a physically grounded quantification of emergency operability, offering quantitative operational insights for emergency scheduling and resilience-oriented decision-making in natural gas pipeline systems.

1. Introduction

As a pivotal transition fuel in the global low-carbon strategy, natural gas plays an indispensable role in supporting power peak regulation, safeguarding urban energy security, and buffering the intermittency of renewable energy. With the deepening coupling of electricity-gas systems (Ameli et al., 2017) and the continuous expansion of cross-regional long-distance pipeline networks, the systemic importance of natural gas infrastructure within integrated energy systems (IES) has increased significantly (Raheli et al., 2025). Meanwhile, the vulnerability of gas pipeline infrastructure to high-impact, low-probability (HILP) events has become increasingly evident (Sesini et al., 2022). Recent representative incidents have underscored the practical urgency of this issue. Geopolitical conflicts (Schill et al., 2025) trigger abrupt supply interruptions, while climate-driven load surges (Li et al., 2022) force pipelines to operate near their physical limits. Such

* Corresponding author.
** Corresponding author.
E-mail addresses: zuolili@cup.edu.cn (L.-L. Zuo), wucc@cup.edu.cn (C.-C. Wu).
Peer review under the responsibility of China University of Petroleum (Beijing).

https://doi.org/10.1016/j.petsci.2026.05.045
1995-8226/

Nomenclature

Sets and vectors

$\mathscr{C}$	Set of compressor stations
$\mathscr{C}_{\mathrm{elec}}$	Set of electric-driven units
$\mathscr{C}_{\mathrm{gas}}$	Set of gas-driven units
$\mathscr{C}_{\mathrm{in}}(i)$	Set of compressor stations flowing into node i
$\mathscr{C}_{\mathrm{out}}(i)$	Set of compressor stations flowing out of node i
$\mathscr{K}$	Set of pipe segments
$\mathscr{K}_{\mathrm{in}}(i)$	Set of pipe segments flowing into node i
$\mathscr{K}_{\mathrm{out}}(i)$	Set of pipe segments flowing out of node i
$\mathscr{N}$	Set of nodes
$\mathscr{N}_{\mathrm{sup}}$	Set of all gas source nodes possessing supply capabilities
$\mathscr{U}$	Set of five typical user types potentially present in the system
$\mathbf{u}$	Vector of system decision variables
$\mathbf{x}$	Vector of system state variables
Ω	Feasible domain defined by system constraints

Parameters

a	Speed of sound, m/s
a_0, a_1, a_2	Polynomial fitting coefficients for head–speed–flow characteristic curve of the compressor
A_k	Cross-sectional area of pipe segment, m^2
b_0, b_1, b_2	Polynomial fitting coefficients for efficient–speed–flow characteristic curve of the compressor
c_0, c_1, c_2	Polynomial fitting coefficients for surge curve of the compressor
d_0, d_1, d_2	Polynomial fitting coefficients for choke curve of the compressor
d_k	Diameter of pipe segment k, m
$D_{i,u,t}^{\mathrm{forecast}}$	Predicted demand of user type u at node i at time t, Nm^3/s
g	Gravitational acceleration, typically taken as 9.81 m/s^2
k_{t}	Temperature heat capacity ratios
k_{v}	Volume heat capacity ratios
LHV	Lower heating value of natural gas, kJ/m^3
n_c	Number of active compressor units within the station
P_{std}	Pressure under standard conditions, Pa
P_i^{lb}	Lower bound of pressure at node i, Pa
P_i^{ub}	Upper bound of pressure at node i, Pa
$Q_{i,\max}^{\mathrm{rate}}$	Maximum allowable instantaneous supply rate at source node i, Nm^3/s
Q_i^{daily}	Maximum allowable daily supply at source node i, Nm^3/d
R	The gas constant, J/(kg·K)
$R_{\mathrm{up},i}$	Maximum allowable ramp-up rates for various gas sources, kg/s
$R_{\mathrm{up},u}$	Maximum allowable shedding rates for user u, Nm^3/s
$R_{\mathrm{down},i}$	Maximum allowable ramp-down rates for various gas sources, kg/s
$R_{\mathrm{down},u}$	Maximum allowable restoration rates for user u, Nm^3/s
$s_{c,t,0}$	Rated rotational speed of the compressors at station c, r/min
$s_{c,t}^{\mathrm{ub}}$	Upper bound of speeds for the compressors at station c at time t, r/min
$s_{c,t}^{\mathrm{lb}}$	Lower bound of speeds for the compressors at station c at time t, r/min
T	System temperature, K
T_{std}	Temperature under standard conditions, K
V_k	Geometric volume of the pipe segment k, m^3
W_u	Shedding priority weight for user type u
ξ	The penalty factor
ρ_{std}	Density under standard conditions, kg/Nm^3
α_u	Maximum allowable shedding coefficient for user u
β	System disturbance factor
η_{m}	Mechanic efficiency of the individual compressors at station c at time t
Δt	Time step size, s
$\Delta t_{\mathrm{delay}}$	The comprehensive response delay time
Δx	Length of the pipe segment, m

Variables

$f_{c,g}$	Fuel gas consumption rate of the station at time t, Nm^3/s
$F_{i,t}^{\mathrm{in}}$	Mass flow rate injected into the pipeline system at node i at time t, kg/s
$F_{i,t}^{\mathrm{out}}$	Mass flow rate withdrawn from the pipeline system at node i at time t, kg/s
$H_{c,t}$	Polytropic head provided by compressor station c at time t, kJ/kg
$\mathrm{LP}_{k,t}$	Linepack of pipe segment k at time t, Nm^3
$M_{k,i,t}$	Mass flow rate at node i within pipe segment k at time t, kg/s
$M_{c,i,t}$	Mass flow rate at node i for compressor station c at time t, kg/s
$\Delta M_{k,t}^{\mathrm{net}}$	Net inflow mass flow rate within pipe segment k at time t, kg/s
$P_{i,t}$	Pressure at node i at time t, Pa
$P_{k,t}^{\mathrm{avg}}$	Average pressure of pipe segment k at time t, Pa
$q_{c,t}$	Actual volumetric flow rate flowing into the compressor at station c at time t, m^3/s
$q_{c,t}^{\max}$	Surge flow limit for the compressors at station c at time t, m^3/s
$q_{c,t}^{\min}$	Choke flow limit for the compressors at station c at time t, m^3/s
$Q_{c,t}$	Volumetric flow rate flowing into the compressor under standard conditions at station c at time t, Nm^3/s
$Q_{\mathrm{cut},i,u,t}$	Shedding flow rate for user u at node i at time t, Nm^3/s
$s_{c,t}$	Rotational speed of the compressors at station c at time t, r/min
Δt_{sur}	System survival time, h
Z	Gas compressibility factor
λ	Hydraulic friction coefficient of pipe segment
$\eta_{c,t}$	Efficiency of the compressors at station c at time t
$\delta_{i,t}$	Slack variable for pressure violations below the minimum limit at node i at time t, Pa
$\Lambda_{\max}$	System resilience limit

disturbances, characterized by rapid propagation and high destructive intensity, far exceed the scope of traditional steady-state reliability assumptions. Consequently, shifting the operational paradigm from static reliability to resilience-oriented dynamic control has emerged as a shared priority for both operators and researchers.

While resilience in natural gas pipeline systems has traditionally been evaluated from a static structural perspective, achieving dynamic operational resilience requires integrating active scheduling with transient physical behaviors. To map this transition, existing studies are reviewed across three interconnected domains. The first category focuses on topological vulnerability. To evaluate network connectivity and structural bottlenecks, recent studies have analyzed structural redundancy and robustness based on complex network theory (Ye et al., 2022), optimized connectivity reliability using minimum path sets and adaptive algorithms (Yang et al., 2025), and assessed network recovery from a cyber-physical perspective considering SCADA communication delays (Marino and Zio, 2021). Furthermore, a multi-dimensional metric framework was proposed by Yang et al. to identify critical nodes under different disturbance types by integrating maximum flow and shortest path algorithms (Yang et al., 2023). Building on this perspective, further research has explored resilience enhancement pathways from an infrastructure planning standpoint. By treating underground gas storage (UGS) facilities as key buffer resources, these studies simulate failure scenarios to evaluate the efficiency and construction priority of different UGS sites in mitigating regional supply shortages (Senderov et al., 2022). While effective for macroscopic planning, the above studies at the topological and structural levels typically neglect the hydraulic constraints compressible gas dynamics, failing to capture the system's actual delivery capability.

The second category centers on operational optimization and scheduling strategies aimed at enhancing efficiency, minimizing energy consumption, and ensuring hydraulic feasibility under both normal and emergency states. Based on mixed-integer linear or nonlinear programming models, extensive strategies have been developed to address specific operational objectives. For normal economic operations, optimization models have been formulated to allocate multi-energy gas supplies for carbon emission reduction (Liu et al., 2022), coordinate load distribution among differently driven compressors to minimize energy consumption (Zhao et al., 2026). Under emergency conditions, operational approaches have focused on underground storage peak-shaving (Senderov et al., 2022), or to ensure maximal load delivery during multi-contingency network disruptions (Tasseff et al., 2022). Some incorporate stochastic (Zhao et al., 2025) or robust programming (Meng et al., 2022) to characterize demand uncertainty or coordinate resilience resources (e.g., linepack and compressor flexibility) within integrated energy systems (Qin et al., 2025). However, most of these studies rely on steady-state assumptions, implicitly assuming instantaneous supply-demand equilibrium. By neglecting the buffering window provided by linepack dynamics, they inevitably underestimate the system's transient carrying capacity under sudden shocks.

The third category focuses on the simulation and mechanistic analysis of transient hydraulics. At the fundamental modeling level, recent studies have evaluated the performance of different numerical algorithms (Koo, 2022) and developed non-isothermal models to capture complex thermodynamic variations (Jia et al., 2025). To reduce computational complexity, interpretable machine learning has also been introduced as an efficient alternative (Zhou et al., 2022). From an operational perspective, dynamic simulations have been further applied to multi-period supply-demand balancing (Wen et al., 2023) and transient peak-shaving under demand uncertainty (Chen et al., 2021). These studies have laid a solid foundation for understanding the transient physical behaviors of pipeline systems. However, most of these works center on operational feasibility, control performance, or energy efficiency, and only limited efforts have explicitly linked transient gas flow dynamics with system-level supply resilience metrics. The core challenge lies in the high nonlinearity and spatiotemporal coupling of the partial differential equations (PDEs) governing transient flow. Integrating these complex physical dynamics directly with system-level active decisions (such as priority-based load shedding) creates a highly non-convex and computationally prohibitive optimization problem. To circumvent this, previous works often rely on purely passive simulations. For instance, Su et al. (2022) employed graph theory and state-space models to conduct detailed simulations of dynamic behaviors under supply interruption scenarios, proposing the linepack depletion rate as a resilience indicator.

In summary, existing studies still exhibit three critical limitations when addressing extreme dynamic disturbances in natural gas pipeline systems.

(1) Separation of transient physical dynamics and decision-making: Many existing emergency scheduling models rely on steady-state assumptions, by ignoring the temporal buffering window provided by linepack depletion, these models fail to accurately quantify how decision latency (response delay) nonlinearly amplifies the risk of system failure (Qian et al., 2023).
(2) Neglect of spatial hydraulic effectiveness in load shedding: Existing shedding strategies often rely on static priority weights, shedding the lowest-priority loads first regardless of their spatial locations. However, due to gas friction and transmission delays, shedding a load far upstream may provide severely attenuated pressure relief to critical downstream nodes. By overlooking this spatial hydraulic sensitivity of demand nodes, existing works fail to capture the trade-off between immediate spatial pressure support and nominal priority levels (Yu et al., 2024).
(3) Ambiguous resilience boundaries: There is a lack of rigorous physical indicators to distinguish failure mechanisms. Specifically, the distinction between time-dominated failures (driven by linepack depletion) and space-dominated failures (constrained by transmission bottlenecks) has not been clearly established (Shan et al., 2023).

To address these critical gaps and move beyond traditional static structural assessments, this study focuses specifically on the intersection of operational optimization and transient hydraulics. By bridging the disconnect between active scheduling decisions and dynamic physical behaviors, we establish a comprehensive approach for operational resilience. Herein, operational resilience is explicitly defined as the system's dynamic capability to absorb extreme shocks and sustain critical nodal pressures. By mathematically coupling linepack dynamics with hierarchical defense strategies into a unified transient formulation, this work provides a systematic approach to quantify and optimize this capability. The main contributions are:

(1) Development of a hierarchical resilience defense system: A comprehensive framework integrating passive linepack buffering, active resource compensation, and adaptive priority-based shedding is proposed to mobilize physical endurance and scheduling resources adaptively.
(2) Formulation of a delay-aware transient optimization model: By coupling transient hydraulics with nonlinear

programming, the model rigorously evaluates the system survival time during decision latency and quantifies the nonlinear amplification of hydraulic costs caused by delayed interventions.

(3) Revealing the spatiotemporal decoupling mechanisms of resilience: To mathematically bound this operational resilience, two key metrics, system survival time and resilience limit, are defined. Case studies quantitatively demonstrate that resilience under supply interruptions is governed by linepack inertia (time-domain), whereas resilience under demand surges is constrained by topological bottlenecks (space-domain).

The main structure of the article is as follows: Section 2 analyzes the resilience defense mechanism and defines resilience metrics. Section 3 details the technical modeling, including transient hydraulic formulation and emergency operation optimization. Section 4 presents two case studies applying the proposed approach to reveal the failure mechanisms under supply-side and demand-side disturbances. Finally, Section 5 concludes the paper. The overall research framework is illustrated in Fig. 1.

2. Resilience mechanism and metrics

Under extreme disturbances, the safety of natural gas pipeline systems is governed not by steady-state balance but by the transient capability to absorb shocks and sustain critical functions. Rooted in the foundational frameworks of resilience engineering for delaying failure and avoiding collapse (Patriarca et al., 2018), this operational resilience practically manifests as the ability to sustain service reliability through multi-level regulatory mechanisms as the feasible hydraulic domain contracts (Asadzadeh et al., 2020).

Distinct from structural resilience, which is topology-focused, or component resilience, which is device-focused, this study proposes an operational resilience framework. As illustrated in Fig. 2, the system response is conceptualized as a three-tier defense mechanism: passive buffering, active regulation, and adaptive degradation. These mechanisms are activated hierarchically based on the disturbance intensity and evolution stage.

Passive buffering serves as the foundational physical defense layer of the system. In the initial phase of a disturbance, or during the response delay interval, the system relies on intrinsic linepack to sustain operations. The gas inventory stored within pipelines is mobilized to bridge the supply–demand gap, mitigating pressure violations. This mechanism provides an instantaneous, passive response determined strictly by the system's initial hydraulic state and geometric capacity (Wang et al., 2023), constituting the inherent resilience of the pipeline system. It defines the system's survival time, creating a critical window for subsequent active interventions.

As linepack depletes, the system activates flexible physical resources. This involves adjusting gas source outputs and modulating compressor set-points to improve pressure profiles. Crucially, this stage does not await total linepack exhaustion; rather, it operates within the finite pressure margin preserved by Tier 1. Its effectiveness is constrained by equipment performance envelopes (e.g., surge/choke limits) and their coupling with nonlinear pipeline hydraulics. Therefore, the core imperative of this stage is to exploit the regulation potential of physical facilities

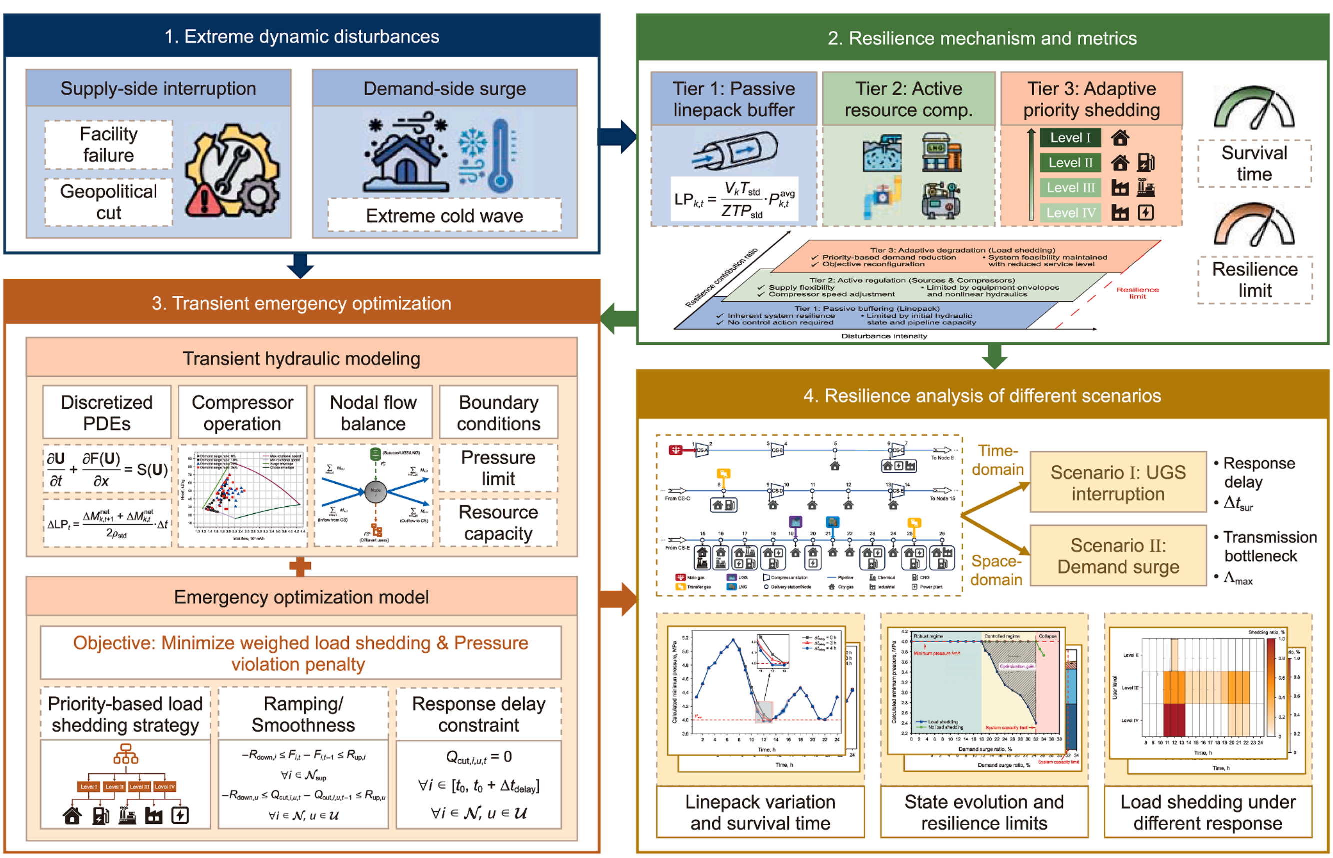

Fig. 1. Overview of the proposed approach.

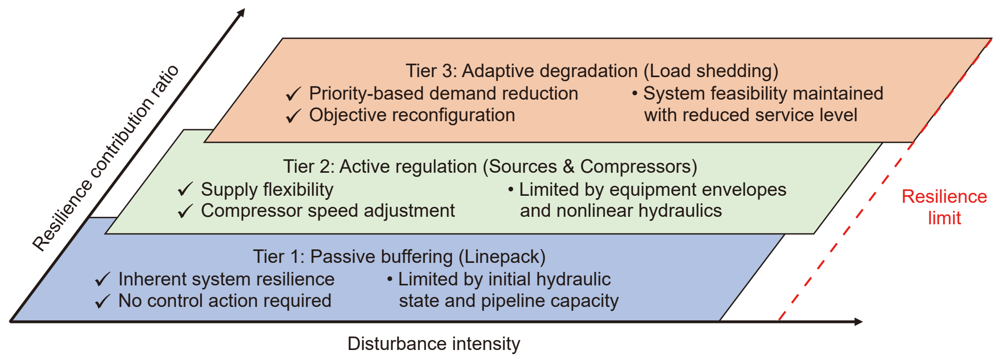

Fig. 2. Three-level resilience defense mechanism.

by leveraging the survival window secured by linepack, demonstrating the system's active capability to withstand sustained disturbances.

When disturbance intensity further escalates and both linepack buffering and physical facility regulation approach their operation limits, the system enters the adaptive degradation stage. To maintain global feasibility, operational objectives are reconfigured by actively load shedding (Malik and Sukhera, 2012). Unlike the previous tiers, this stage sacrifices non-essential loads to protect critical users (e.g., residential sectors) through a priority-based strategy. From a resilience perspective, this represents the optimal feasible state under extreme constraints rather than a control failure.

To quantitatively evaluate the effectiveness of these mechanisms under extreme conditions, this study defines the following resilience metrics across temporal and intensity dimensions:

(1) System survival time

System survival time is defined as the maximum duration, starting from the disturbance onset time t_0, during which the system can maintain all nodal pressures above safety limits without external load shedding interventions, as expressed in Eq. (1). This metric quantifies the temporal buffering capacity synthesized by passive linepack and active regulation, serving as a critical basis for assessing the urgency of emergency response.

$$\Delta t_{\mathrm{sur}} = \max\left\{\tau \middle| P_{i,t} \geq P_i^{\mathrm{lb}}, \forall i \in \mathcal{N}, t \in [t_0, t_0+\tau] \right\} \tag{1}$$

where Δt_{sur} denotes the system survival time, h; $P_{i,t}$ denotes the pressure at node i at time t, Pa; P_i^{lb} denotes the lower bound pressure at node i, Pa.

(2) Resilience limit

The resilience limit is defined as the maximum disturbance intensity the system can withstand after exhausting all available physical regulation measures and maximizing load shedding strategies. Within this limit, the continuous supply for significant essential users (e.g., residential loads) can be sustained through priority-based shedding. As expressed in Eq. (2), this limit represents the physical boundary of the system dictated by topological transmission bottlenecks or total supply capacity, beyond which no operational strategy can prevent failure.

$$\Lambda_{\max} = \sup\{\beta \geq 0 | \exists(\mathbf{x}, \mathbf{u}) \in \Omega(\beta)\} \tag{2}$$

where $\Lambda_{\max}$ denotes the system resilience limit; $\mathbf{x}$ represents the vector of system state variables (e.g., nodal pressures, pipe flows); $\mathbf{u}$ represents the vector of system decision variables (e.g., compressor ratios, load shedding rates); β represents the system disturbance factor; $\Omega(\beta)$ denotes the feasible domain defined by system physical and operational constraints.

3. Methodology

3.1. Overview and assumptions

This section formulates a transient emergency optimization model. Unlike steady-state approaches, it explicitly characterizes dynamic resilience measures, including linepack buffering, equipment regulation, and priority-based load shedding. To balance computational efficiency with engineering safety during emergency response, the model incorporates the following assumptions based on practical engineering scenarios:

(1) One-dimensional isothermal flow: Given the extremely high length-to-diameter ratio of long-distance pipelines, radial variations in flow parameters are neglected. Assuming sufficient heat exchange between the gas and the surrounding soil, the dynamic impact of temperature gradients along the route is disregarded.
(2) Horizontal pipeline assumption: In high-pressure long-distance transmission systems, pressure losses caused by friction dominate over gravitational potential effects. Elevation changes within the pipeline segments are therefore ignored in this study.
(3) Fixed compressor unit commitment: During the short-term transient response to extreme disturbances (typically within 24 h), the priority is to rapidly mitigate pressure violations rather than reconfiguring unit commitment. Starting up large-scale compressor units involves significant time delays (e.g., purging, warming up) and mechanical risks, which may not match the urgency of the initial emergency response. Therefore, this study assumes the number of active units remains constant, with regulation achieved primarily through rotational speed adjustments. This assumption represents a conservative strategy to ensure operational stability during the critical transient window.

3.2. General transient hydraulic modeling

3.2.1. Pipe segment governing equations

The gas flow within pipelines is governed by the laws of conservation of mass and momentum, typically taking the form of a system of partial differential equations (PDEs) (LeVeque, 1992).

The governing PDEs are discretized using the implicit central difference method. This scheme ensures unconditional numerical stability, allowing for larger time steps adapted to the emergency scheduling horizon while maintaining computational efficiency.

Let $\mathscr{K}$ denotes the set of pipe segments, $\mathscr{N}$ denotes the set of nodes. For any pipe segment k (connecting node i to i+1), the discretized continuity and momentum equations are expressed as Eqs. (3) and (4) (Chen et al., 2021):

$$\frac{P_{i,t+1}+P_{i+1,t+1}-P_{i,t}-P_{i+1,t}}{2\Delta t}+\frac{a^2}{A_k}\cdot\frac{M_{k,i+1,t}+M_{k,i+1,t+1}-M_{k,i,t}-M_{k,i,t+1}}{2\Delta x}=0,\forall i\in\mathscr{N},k\in\mathscr{K} \tag{3}$$

$$\frac{P_{i+1,t}+P_{i+1,t+1}-P_{i,t}-P_{i,t+1}}{2\Delta x}+\frac{1}{A_k}\cdot\left(\frac{M_{k,i,t+1}+M_{k,i+1,t+1}-M_{k,i,t}-M_{k,i+1,t}}{2\Delta t}\right)+\frac{\lambda a^2}{2dA_k^2}\cdot\left(\frac{P_{i,t+1}+P_{i+1,t+1}+P_{i,t}+P_{i+1,t}}{4}\right)^{-1}\cdot\left(\frac{M_{k,i,t+1}+M_{k,i+1,t+1}+M_{k,i,t}+M_{k,i+1,t}}{4}\right)\cdot\left|\frac{M_{k,i,t+1}+M_{k,i+1,t+1}+M_{k,i,t}+M_{k,i+1,t}}{4}\right|=0,\forall i\in\mathscr{N},k\in\mathscr{K} \tag{4}$$

where $M_{k,i,t}$ represents the mass flow rate at node i within pipe segment k at time t, kg/s; a is the speed of sound, m/s; A_k is the cross-sectional area of pipe segment, m^2; d_k is the diameter of pipe segment k, m;λ denotes the hydraulic friction coefficient of pipe segment; Δx represents the length of the pipe segment, corresponding to the discretized spatial step size, m; Δt is the time step size, s.

Under emergency conditions, linepack serves as the primary temporal buffer mechanism against sudden disturbances (Su et al., 2022). To explicitly quantify this buffering effect, the discretized continuity equation is algebraically reformulated. Let $P^{\text{avg}}_{k,t}=0.5(P_{i,t}+P_{i+1,t})$ denotes the average pressure of pipe segment k at time t, and let $\Delta M^{\text{net}}_{k,t}=M_{k,i,t}-M_{k,i+1,t}$ represent the net inflow mass flow rate. With V_k representing the geometric volume of the pipe segment, Eq. (3) can be transformed into Eq. (5).

$$\frac{P^{\text{avg}}_{k,t+1}-P^{\text{avg}}_{k,t}}{\Delta t}=\frac{a^2}{V_k}\cdot\frac{\Delta M^{\text{net}}_{k,t+1}+\Delta M^{\text{net}}_{k,t}}{2},\forall k\in\mathscr{K} \tag{5}$$

Based on the real gas equation of state (EOS) and the definition of linepack, the linepack LP exhibits a linear relationship with the average pressure $P^{\text{avg}}_{k,t}$, expressed as Eq. (6).

$$\text{LP}_{k,t}=\frac{V_kT_{\text{std}}}{ZTP_{\text{std}}}\cdot P^{\text{avg}}_{k,t},\forall k\in\mathscr{K} \tag{6}$$

where Z is the gas compressibility factor. To accurately calculate the compressibility factor and thermodynamic properties under high-pressure operating regimes, the BWRS equation of state is adopted (Ghilardi et al., 2025; Liu et al., 2025), with compositional parameters sourced from standard industrial databases; T denotes the gas temperature, K; P_{std} and T_{std} represent the gas pressure and temperature under standard conditions, adopted as 101325 Pa and 293.15 K, respectively, in this study.

By substituting this relationship into the continuity equation, the linepack state transition constraint is derived, as shown in Eq. (7). This equation indicates that the linepack state at the next time step is strictly determined by the current linepack and the integral of the net mass inflow over the time interval.

$$\text{LP}_{t+1}=\text{LP}_t+\frac{\Delta M^{\text{net}}_{k,t+1}+\Delta M^{\text{net}}_{k,t}}{2\rho_{\text{std}}}\cdot\Delta t,\forall k\in\mathscr{K} \tag{7}$$

where ρ_{std} represents the density under standard conditions, kg/Nm^3.

3.2.2. Compressor station operational constraints

Centrifugal compressor units exhibit highly nonlinear off-design characteristics. Their operational states are subject to the dual constraints of thermodynamic laws and mechanical performance limits, while exhibiting distinct energy-mass coupling behaviors depending on the driver type. Let the set of compressor stations in the system be denoted as $\mathscr{C}$, which is further divided into the set of gas-driven units $\mathscr{C}_{\text{gas}}$ and the set of electric-driven units $\mathscr{C}_{\text{elec}}$, with $\mathscr{C}=\mathscr{C}_{\text{gas}}\cup\mathscr{C}_{\text{elec}}$. For a compressor station c whose inlet and outlet nodes are i and i+1, respectively, the polytropic head $H_{c,t}$ provided by the unit must satisfy the thermodynamic relationship of the polytropic process, expressed by Eq. (8).

$$H_{c,t}=\frac{k_{\text{v}}}{k_{\text{v}}-1}Z_{i,t}RT_{i,t}\cdot\left[\left(\frac{P_{i+1,t}}{P_{i,t}}\right)^{\frac{k_{\text{t}}-1}{k_{\text{t}}}}-1\right],\forall c\in\mathscr{C} \tag{8}$$

where k_{v} and k_{t} denote the volume and temperature heat capacity ratios, respectively; R is the gas constant, J/(kg·K).

Compressor units within each station are required to operate strictly within their performance envelopes. In this study, polynomial fitting is employed to approximate the various operational envelopes. The corresponding constraints, formulated based on the actual volumetric inlet flow and rotational speed under operating conditions, are presented in Eqs. (9)–(14) (Zhao et al., 2026). These constraints are used to describe the rapid regulation capability of compressors following disturbances, forming an essential physical basis for system recovery capability.

$$H_{c,t}=a_0\cdot\frac{s^2_{c,t}}{s^2_{c,t,0}}+a_1\cdot q_{c,t}\cdot\frac{s_{c,t}}{s_{c,t,0}}+a_2\cdot q^2_{c,t},\forall c\in\mathscr{C} \tag{9}$$

$$\eta_{c,t}=b_0+b_1\cdot q_{c,t}\cdot\frac{s_{c,t,0}}{s_{c,t}}+b_2\cdot\frac{s^2_{c,t,0}}{s^2_{c,t}}\cdot q^2_{c,t},\forall c\in\mathscr{C} \tag{10}$$

$$q^{\min}_{c,t}=c_0+c_1\cdot s_{c,t}+c_2\cdot s^2_{c,t},\forall c\in\mathscr{C} \tag{11}$$

$$q^{\max}_{c,t}=d_0+d_1\cdot s_{c,t}+d_2\cdot s^2_{c,t},\forall c\in\mathscr{C} \tag{12}$$

$$q^{\min}_{c,t}\le q_{c,t}\le q^{\max}_{c,t},\forall c\in\mathscr{C} \tag{13}$$

$$s_{c,t}^{\mathrm{lb}} \le s_{c,t} \le s_{c,t}^{\mathrm{ub}}, \forall c \in \mathscr{C} \tag{14}$$

where $q_{c,t}$ denotes the actual volumetric inlet flow rate flowing into the compressor at station c at time t, m^3/s; $s_{c,t}$ represents the rotational speed of the compressors at station c at time t, r/min; $s_{c,t,0}$ denotes the rated rotational speed of the compressors at station c; $\eta_{c,t}$ represents the efficiency of the compressors at station c at time t; $q_{c,t}^{\max}$ and $q_{c,t}^{\min}$ denote the surge flow limit and choke (stonewall) flow limit, respectively, for the compressors at station c at time t, m^3/s; $s_{c,t}^{\mathrm{ub}}$ and $s_{c,t}^{\mathrm{lb}}$ represent the upper bound and lower bound of rotational speeds allowed for the compressors at station c at time t; a_0, a_1, a_2, b_0, b_1, b_2, c_0, c_1, c_2, d_0, d_1, d_2 are the polynomial fitting coefficients.

The mass flow balance within a compressor station is contingent upon the driver configuration of the compressor units. Eqs. (15) and (16) formulate the flow balance constraints for stations equipped with electric-driven and gas-driven units, respectively.

$$M_{c,i,t} = M_{c,i+1,t} = n_c \rho_{\mathrm{std}} Q_{c,t}, \forall c \in \mathscr{C}_{\mathrm{elec}} \tag{15}$$

$$M_{c,i,t} = M_{c,i+1,t} + n_c \rho_{\mathrm{std}} f_{c,\mathrm{g}} = n_c \rho_{\mathrm{std}} \cdot \left(Q_{c,t} + f_{c,\mathrm{g}}\right), \forall c \in \mathscr{C}_{\mathrm{gas}} \tag{16}$$

where $M_{c,i,t}$ represents the mass flow rate at node i for compressor station c at time t, kg/s; n_c denotes the number of active compressor units within the station; $Q_{c,t}$ represents the volumetric flow rate flowing into the compressor under standard conditions at station c at time t, Nm^3/s; $f_{c,\mathrm{g}}$ denotes the fuel gas consumption rate of the station at time t, which can be calculated via Eq. (17).

$$f_{c,\mathrm{g}} = H_{c,t} \frac{Q_{c,t} \rho_{\mathrm{std}}}{\eta_{c,t} \eta_{\mathrm{m}} \cdot \mathrm{LHV}}, \forall c \in \mathscr{C}_{\mathrm{gas}} \tag{17}$$

where η_{m} represents the mechanic efficiency of the individual compressors at station c at time t; LHV represents the lower heating value of natural gas, $\mathrm{kJ/m}^3$.

3.2.3. Nodal flow balance

The pipe segment equations describe only the internal transmission behavior of gas within individual pipes. To couple the hydraulic dynamics with system topology and external supply–demand interactions, a mass balance equation is formulated for each node i within the system. As illustrated in Fig. 3, for any arbitrary node i, the flow balance constraint at time t is expressed as Eq. (18).

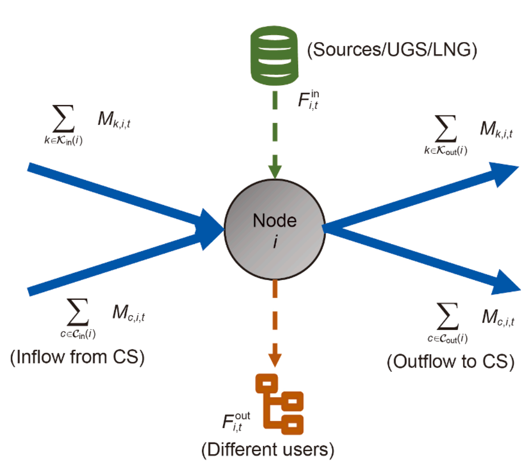

Fig. 3. Nodal flow balance.

$$\begin{aligned} &\sum_{k\in\mathscr{K}_{\mathrm{in}}(i)} M_{k,i,t} + \sum_{c\in\mathscr{C}_{\mathrm{in}}(i)} M_{c,i,t} + F_{i,t}^{\mathrm{in}} - \\ &\left(\sum_{k\in\mathscr{K}_{\mathrm{out}}(i)} M_{k,i,t} + \sum_{c\in\mathscr{C}_{\mathrm{out}}(i)} M_{c,i,t} + F_{i,t}^{\mathrm{out}}\right) = 0, \forall i \in \mathscr{N} \end{aligned} \tag{18}$$

where $\mathscr{K}_{\mathrm{in}}(i)$ and $\mathscr{K}_{\mathrm{out}}(i)$ denote the sets of pipe segments flowing into and out of node i, respectively; $\mathscr{C}_{\mathrm{in}}(i)$ and $\mathscr{C}_{\mathrm{out}}(i)$ denote the sets of compressor stations flowing into and out of node i, respectively; $F_{i,t}^{\mathrm{in}}$ represents the mass flow rate injected into the pipeline system at node i (e.g., from UGS or LNG terminals) at time t, kg/s; $F_{i,t}^{\mathrm{out}}$ represents the mass flow rate withdrawn from the pipeline system at node i (e.g., for distribution users) at time t, kg/s.

3.2.4. Boundary conditions & resource constraints

(1) Resource capacity constraints

Pipeline systems typically integrate multiple types of supply sources, including pipeline gas (originating from upstream gas fields or transfers from interconnecting pipelines), UGS facilities utilized for peak shaving, and LNG receiving terminals. These sources differ in both physical characteristics and operational limitations. To provide a unified description of supply characteristics across various sources, let $\mathscr{N}_{\mathrm{sup}}$ denote the set of all gas source nodes possessing supply capabilities within the system. During peak periods, the operation of source nodes must simultaneously satisfy the physical limits of instantaneous supply rates and the contractual limits regarding total daily supply, as formulated in Eqs. (19) and (20).

$$0 \le F_{i,t}^{\mathrm{in}} \le Q_{i,\max}^{\mathrm{rate}} \cdot \rho_{\mathrm{std}}, \forall i \in \mathscr{N}_{\mathrm{sup}} \tag{19}$$

$$\sum_{t=1}^{T} F_{i,t}^{\mathrm{in}} \cdot \Delta t \le Q_i^{\mathrm{daily}} \cdot \rho_{\mathrm{std}}, \forall i \in \mathscr{N}_{\mathrm{sup}} \tag{20}$$

where $Q_{i,\max}^{\mathrm{rate}}$ denotes the maximum allowable instantaneous supply rate at source node i, Nm^3/s; Q_i^{daily} denotes the maximum allowable daily supply at source node i, Nm^3/d.

(2) Nodal pressure safety boundary

Constrained by the design pressure of the pipelines, the pressure at every node must adhere to a corresponding upper limit. Simultaneously, the pressure supplied to each user must satisfy specific delivery pressure requirements, as formulated in Eq. (21).

$$P_i^{\mathrm{lb}} \le P_{i,t} \le P_i^{\mathrm{ub}}, \forall i \in \mathscr{N} \tag{21}$$

where P_i^{ub} denotes the upper bound pressure at node i, Pa.

3.3. Emergency optimization model under extreme conditions

Building upon the general transient hydraulic model established in Section 3.2, this section introduces emergency shedding decision variables and a priority-based mechanism to address extreme disturbance scenarios during peak supply periods.

Table 1
User priority levels and shedding coefficients.

Priority level	Description	Typical user category	Max shedding coefficient
I. Fully protected	Rigid load. Critical for public livelihood and social stability; shedding is strictly prohibited.	City gas (Residential/Public service sectors)	0%
II. Minimally sheddable	Quasi-rigid load. Short-term or minor shedding is permissible only under extreme crises.	CNG, City gas (Commercial sector)	10%–30%
III. Sheddable	Elastic load. Production processes allow for load regulation; significant shedding is permissible.	General industrial, Chemical	50%–80%
IV. Interruptible	Peak-shaving load. Users with alternative fuel sources or signed interruptible contracts; complete shedding is permissible.	Power plants (Dual-fuel), Specific industrial users	100%

3.3.1. *Priority-based load shedding strategy*

To ensure public safety and minimize social impact under supply shortages, a structured mapping between user types and supply priority levels is established. Let $\mathscr{U} = \{\text{City gas, CNG, Industrial, Chemical, Power plant}\}$ denote the set of five typical user types potentially present in the system. Based on the socioeconomic importance and process characteristics of each user, and considering the differences in safety risks and economic losses associated with supply interruption, a four-level security strategy is formulated (Huang et al., 2021). Each level corresponds to a specific maximum allowable shedding coefficient α_u, as detailed in Table 1.

Based on Table 1, the constraints for user load shedding are formulated. Let $D_{i,u,t}^{\text{forecast}}$ denote the predicted demand (under standard conditions) of user type u at node i at time t. A decision variable $Q_{\text{cut},i,u,t}$ is introduced to represent the shedding flow rate for this specific user type. Consequently, the shedding flowrate at any instant is constrained by both the user's physical demand upper bound and their corresponding priority level, as formulated in Eq. (22).

$$0 \le Q_{\text{cut},i,u,t} \le \alpha_u \cdot D_{i,u,t}^{\text{forecast}}, \forall i \in \mathscr{N}, u \in \mathscr{U} \tag{22}$$

In practical pipeline operations, a single delivery station typically supplies multiple types of downstream users simultaneously, resulting in significant compositional complexity of the nodal load. To achieve precise regulation extending from macroscopic nodal aggregates to microscopic user types, a nodal load model based on user composition is established. The nodal withdrawal mass flow rate $F_{i,t}^{\text{out}}$ defined in the hydraulic model (see Section 3.2.3) essentially represents the aggregate of the actual gas consumption of various user types at that node. The relationship between them is expressed as Eq. (23).

$$F_{i,t}^{\text{out}} = \sum_{u \in \mathscr{U}} \left(D_{i,u,t}^{\text{forecast}} - Q_{\text{cut},i,u,t} \right) \cdot \rho_{\text{std}}, \forall i \in \mathscr{N} \tag{23}$$

3.3.2. *Emergency operational constraints*

(1) Load shedding response delay

Emergency response involves inherent latencies due to fault diagnosis and decision transmission. Let Δt_{delay} denote the comprehensive response delay. During this interval, load shedding is strictly prohibited (see Eq. (24)), forcing the system to rely exclusively on linepack buffering and active regulation. Consequently, the no-load-shedding interval imposed by this delay constraint serves as the direct basis for evaluating the system survival time defined in Eq. (1). If the response delay exceeds the system's survival time, the pressure limits will be irreversibly breached before any load shedding intervention can take effect.

$$Q_{\text{cut},i,u,t} = 0, \forall t \in \left[t_0, t_0 + \Delta t_{\text{delay}} \right], \forall i \in \mathscr{N}, u \in \mathscr{U} \tag{24}$$

(2) Operational smoothness

To ensure the mechanical safety of regulators and avoid downstream pressure oscillations, ramping constraints are imposed on both supply adjustment and load shedding recovery, as formulated in Eqs. (25) and (26). Let $R_{\text{up},i}$ and $R_{\text{down},i}$ denote the maximum allowable ramp-up and ramp-down rates for various gas sources, $R_{\text{up},u}$ and $R_{\text{down},u}$ denote the maximum allowable shedding and restoration rates for user u.

$$-R_{\text{down},i} \le F_{i,t} - F_{i,t-1} \le R_{\text{up},i}, \forall i \in \mathscr{N}_{\text{sup}} \tag{25}$$

$$-R_{\text{down},u} \le Q_{\text{cut},i,u,t} - Q_{\text{cut},i,u,t-1} \le R_{\text{up},u}, \forall i \in \mathscr{N}, u \in \mathscr{U} \tag{26}$$

(3) Nodal pressure violation penalty

To prevent mathematical infeasibility under extreme physical deficits, the rigid lower pressure bound is relaxed using non-negative slack variables, as formulated in Eq. (27). This formulation characterizes the magnitude of pressure violations, prioritizing the minimization of violation severity over simple feasibility checks.

$$P_{i,t} + \delta_{i,t} \ge P_i^{\text{lb}}, \forall i \in \mathscr{N} \tag{27}$$

where $\delta_{i,t}$ represents the slack variable for pressure violations below the minimum limit at node i at time t.

3.3.3. *Optimization objective*

Under extreme operating conditions, the core objective of emergency scheduling in pipeline systems is to minimize the weighted social supply shortage loss. Considering the disparities in the unit economic value of gas shortages and the social impacts across different user types, a hierarchical weighting system is constructed. The total objective function J comprises a socio-economic loss term and a pressure violation penalty term, as expressed in Eq. (28).

$$\min J = \sum_{t=1}^{T} \sum_{i \in \mathcal{N}} \sum_{u \in \mathcal{U}} W_u \cdot Q_{\text{cut},i,u,t} \cdot \Delta t + \sum_{t=1}^{T} \sum_{i \in \mathcal{N}} \xi \cdot \delta_{i,t} \tag{28}$$

where W_u denotes the shedding priority weight for user type u; ξ represents the penalty factor.

The assignment of priority weights W_u is primarily based on the heterogeneity of social impact as well as the need to guide the numerical search direction of the optimization. Residential and public-service gas users are closely related to public safety and social stability, they are assigned significantly higher weights. In contrast, industrial and power generation users mainly incur economic losses and generally possess stronger operational flexibility or buffering capacity, and thus receive relatively lower weights. This differential weight setting steers the optimization algorithm to follow the minimum-cost path during the search process.

3.3.4. Formulation summary

In summary, the emergency operation optimization problem for natural gas pipeline systems under extreme conditions can be formulated as the following NLP model, as presented in Eq. (29).

$$\min \quad \text{objective function} : \text{Eq. (28)} \tag{29a}$$

$$\text{s.t.} \quad \text{Hydraulic physics} : \text{Eqs. (3)–(4)} \tag{29b}$$

$$\text{Compressor station operation constraints} : \text{Eqs. (8)–(17)} \tag{29c}$$

$$\text{Nodal flow balance} : \text{Eq. (18), Eq. (23)} \tag{29d}$$

$$\text{Source constraints} : \text{Eqs. (19)–(20)} \tag{29e}$$

$$\text{Node pressure limits} : \text{Eq. (21), (27)} \tag{29f}$$

$$\text{Emergency operational constraints} : \text{Eqs. (24)–(26)} \tag{29g}$$

4. Case study

The emergency optimization model is implemented in Python using the Pyomo framework and solved via the IPOPT solver, chosen for its robustness in handling large-scale sparse nonlinear problems (Wächter and Biegler, 2006). The optimization is solved on a laptop equipped with an Intel Core i5 processor and 16 GB RAM. For the tested system comprising 26 nodes and 39 demand units, with a simulation horizon of 24 h and a time step of 1 h, the average computation time for each scenario is approximately 40 s, satisfying the timeliness requirement for emergency decision-making.

4.1. Case description

The study focuses on a typical long-distance high-pressure pipeline system with multi-source joint supply (Fig. 4). The topology comprises five supply sources (one main pipeline, two transfer stations, one LNG terminal, and one UGS facility) and five compressor stations. Key physical parameters are detailed in Table 2.

The system serves 39 independent users across 19 delivery stations. These users cover the five typical user types defined previously. The baseline load profiles of all delivery users are selected based on a representative winter day operating condition. Among them, rigid city gas loads account for approximately 60% of the total demand. Differentiated priority weights and maximum shedding ratios are assigned accordingly, as presented in Appendix Table A1.

To comprehensively evaluate the performance of the proposed model, two extreme scenarios are designed. The simulation horizon is 24 h, with a time step of 1 h. A sensitivity analysis on the time step (15 min, 30 min, and 1 h) was conducted, as detailed in Appendix Table A.2. The results confirm that the 1-h interval accurately captures the transient dynamics and system survival time, and strictly aligns with the practical operational frequency of real-world dispatch centers, while maintaining high computational efficiency. Scenario 1 considers a sudden UGS failure occurring at

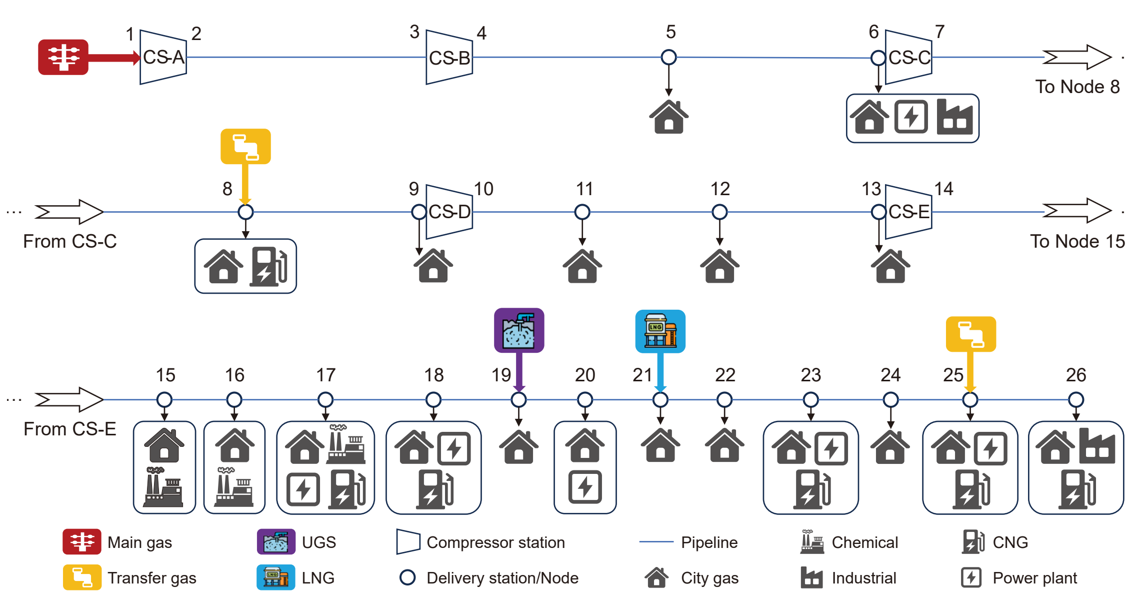

Fig. 4. Topology of the pipeline system.

Table 2
The key physical parameters of the system.

Category	Item	Value	Unit
Pipeline	Diameter	963.6–981	mm
	Length	7.15–152.3	km
	Roughness	0.02	mm
	Design pressure	10	MPa
Compressor station	Numbers of running compressor	[1,1,1,1,1]	
	Rotational speed range	A: [2880,5040]; B: [3660,6405]; C: [2880,5040]; D: [3000,5250]; E: [3660,6405]	r/min
	Motor type	[Electric, Gas, Electric, Electric, Gas]	
Operational conditions	Minimum allowable nodal pressure	4	MPa
	Main supply pressure	Fixed at 6 MPa for main gas	
	Node supply capacity	Node 1: 3600; Node 8: 550; Node 19: 750; Node 21: 1400; Node 25: 1060	10^4 m^3/d

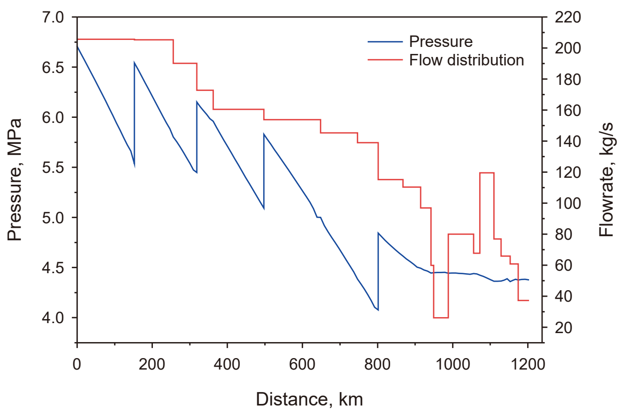

Fig. 5. The resulting initial nodal pressures and flow distributions.

08:00 during the morning peak, focusing on temporal response capabilities under varying decision delays ($\Delta t_{\text{delay}} = 0$–4 h). Scenario 2 considers a cold-wave-induced surge in gas demand, emphasizing the model's spatial scheduling capability and resilience limit. Under this condition, system-wide demand increases with different ratios (0%–35%). For both scenarios, the initial conditions are derived by solving a steady-state operation optimization model based on the flow rates at each delivery station at 00:00. The resulting initial nodal pressures and flow distributions are detailed in Fig. 5. Furthermore, the baseline daily demand curves for different types of users are presented in Fig. 6.

4.2. Results and discussion

4.2.1. Scenario 1

Fig. 7 illustrates the system's dynamic evolution under varying response delays ($\Delta t_{\text{delay}} = 0$–4 h), where Fig. 7(a) presents the time variation of the terminal pressure, reflecting the minimum pressure level within the system, while Fig. 7(b) tracks the total linepack inventory.

Prior to the incident, the system accumulates gas inventory during the nocturnal low-demand period, establishing a sufficient hydraulic buffer. Following the sudden UGS interruption at 08:00, which coincides with the morning peak ramping, a severe supply deficit emerges. Consequently, both the terminal node pressure and total linepack inventory exhibit a rapid decline.

As observed in Fig. 7(a), extending the response delay from 0 h to 3 h pushes the system toward its physical resilience limit. When $\Delta t_{\text{delay}} = 3$ h, intensive load shedding initiated at $t = 11$ h barely succeeds in arresting the pressure decay, maintaining the minimum pressure just above the 4.0 MPa safety threshold. In stark contrast, when the delay reaches 4 h, the intervention comes too late. The accumulated hydraulic deficit becomes unrecoverable, causing the pressure to irreversibly breach the safety limit at $t = 12$ h. Crucially, this bifurcation quantifies the system survival time Δt_{sur} defined in Eq. (1). The results indicate that under this specific interruption scenario, the system's intrinsic survival time lies strictly within the interval of 3 h < Δt_{sur} < 4 h. This value represents the maximum decision latency allowable before the system loses its hydraulic recoverability.

A comparison between Fig. 7(a) and (b) further reveals that the linepack acts as a finite temporal buffer; once this buffer is depleted beyond a critical point, the hydraulic cost to restore pressure escalates disproportionately, rendering subsequent interventions ineffective. This result confirms that linepack functions as an accumulated buffering resource for system resilience, while pressure serves as an instantaneous indicator.

After the response delay period ends and load shedding measures are activated, the recovery trajectories gradually converge across different cases. This indicates that response delay primarily affects the system survival time during the disturbance stage, whereas the final recovery capability is largely determined by physical infrastructure capacity and shows limited dependence on the preceding response history.

To further quantify the impact of response speed on service levels, Fig. 8 utilizes spatiotemporal heat maps to compare the load shedding distribution between the no-delay ($\Delta t_{\text{delay}} = 0$ h) and critical response ($\Delta t_{\text{delay}} = 3$ h) scenarios. Since Level I users are fully protected throughout the process, their shedding results are not presented.

In the immediate response case ($\Delta t_{\text{delay}} = 0$ h), shedding is distributed across a broad time window (08:00–22:00), allowing for a lower instantaneous shedding intensity by leveraging the combined effect of linepack and mild demand reduction. Conversely, under the critical delay scenario ($\Delta t_{\text{delay}} = 3$ h), the system is forced to concentrate the shedding volume within a narrowed window to compensate for the deepened deficit. This results in a sharp spike in shedding intensity between 11:00 and 13:00, significantly increasing the instantaneous impact on users.

A critical observation regarding user priority emerges from the spatial distribution of shedding. As indicated in the optimization results, the system prioritizes shedding higher-priority Level III users located at the terminal nodes (e.g., Nodes 23–26) over lower-priority Level IV users situated upstream. This counter-intuitive strategy is governed by spatial hydraulic effectiveness: shedding downstream loads provides immediate and direct pressure relief to the critical

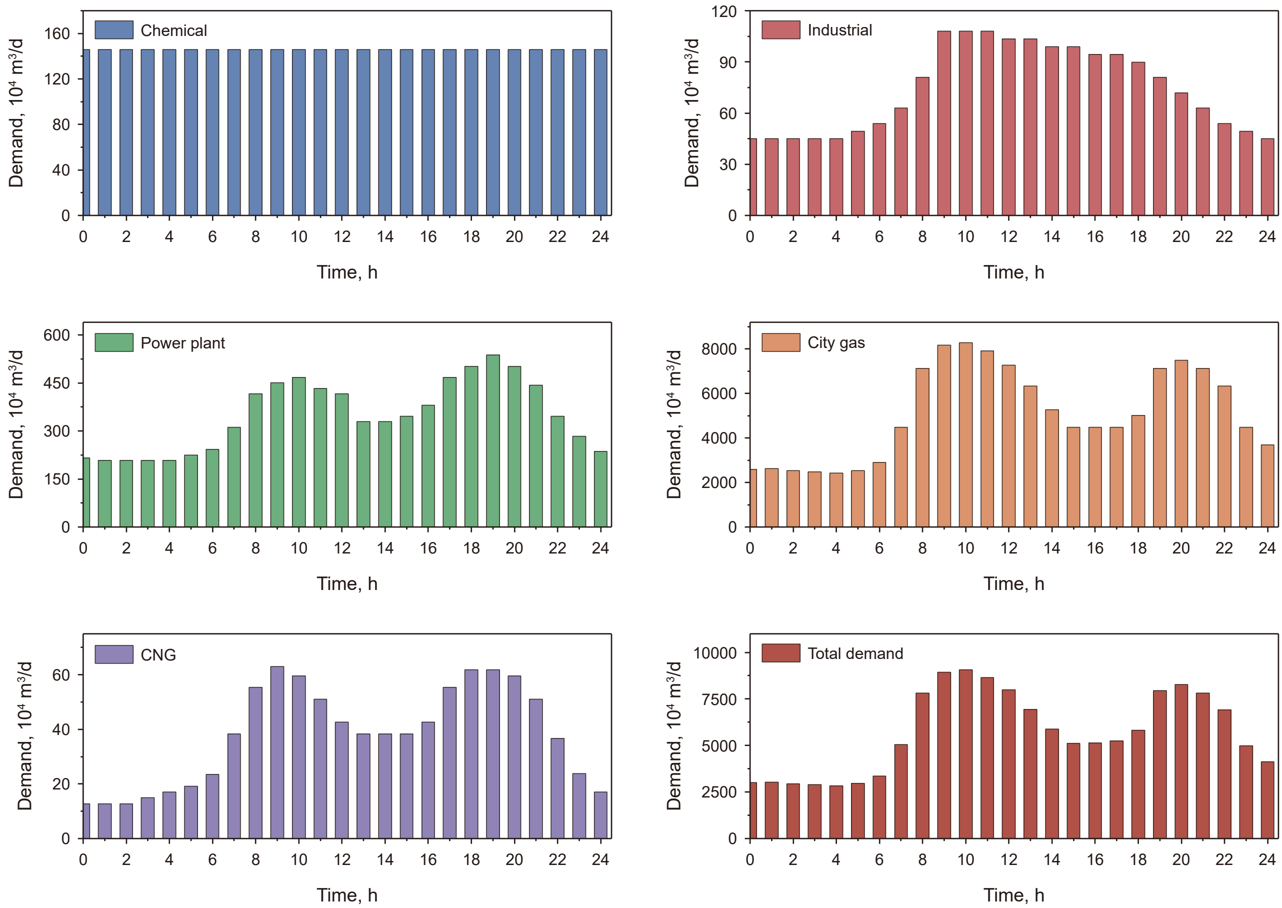

Fig. 6. The baseline daily demand curves for different types of users.

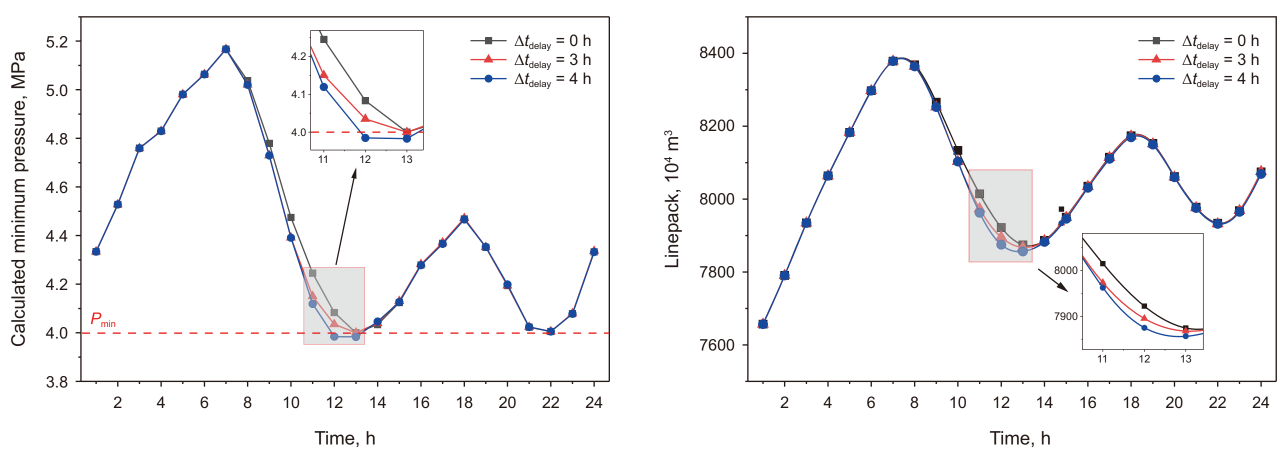

(a) The terminal node pressure

(b) The total linepack

Fig. 7. The system's dynamic evolution under varying response delays.

low-pressure points. In contrast, the pressure recovery potential from upstream shedding is severely attenuated by long-distance frictional losses. This finding underscores that in emergency states, the hydraulic sensitivity of a load's location can outweigh its economic priority, necessitating a spatially aware shedding strategy.

To further demonstrate the overall advancements of the proposed transient approach, a traditional steady-state optimization was evaluated. As detailed in Table 3, the steady-state model strictly enforces instantaneous flow equilibrium, fundamentally failing to capture linepack buffering. Consequently, it calculates a 0-h survival time, triggering total load shedding of 306.83×10^4 m^3. In stark contrast, the transient model dynamically mobilizes linepack, extending the survival window to 3–4 h and reducing total shedding to just 79.68×10^4 m^3. This 74.0% reduction quantitatively confirms the socio-economic necessity of incorporating transient dynamics into emergency decision-making.

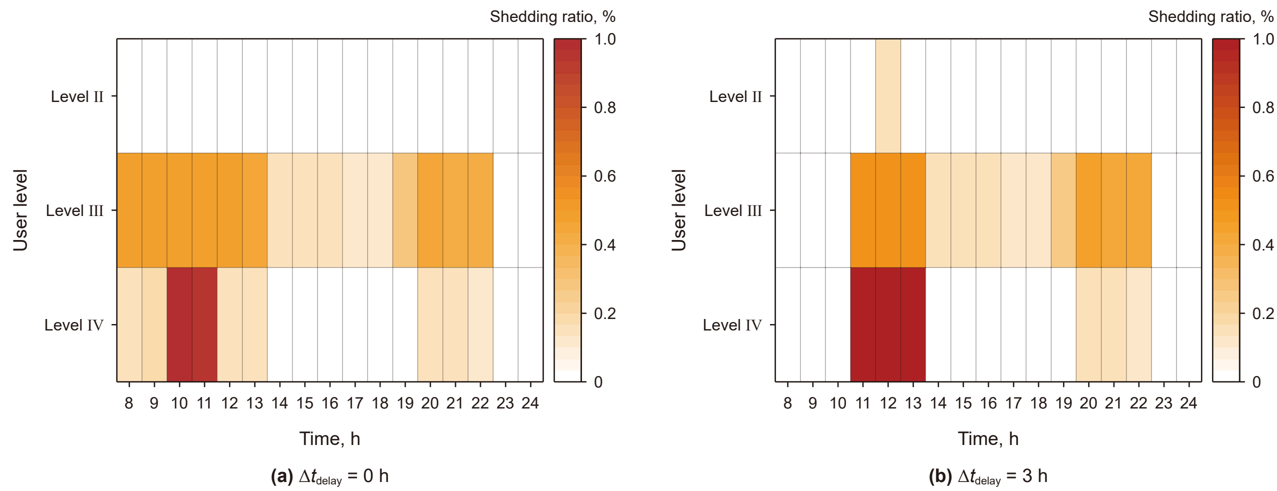

Fig. 8. The load shedding distribution of different response delay time.

Table 3
Comparison of emergency response performance between steady-state and transient models.

Model	System survival time	Total load shedding, 10^4 m^3
Steady-state optimization	0 h	306.83
Transient optimization	3–4 h	79.68

Overall, the results demonstrate that resilience relies on the synergy between intervention timing and linepack inertia. Excessive delay not only shortens the survival window but also fundamentally alters the shedding structure, shifting operational risk toward higher-priority users. Therefore, emergency scheduling must balance hydraulic security and social cost by actively utilizing the limited decision window provided by linepack dynamics.

4.2.2. Scenario 2

Distinct from the supply-side failure in Scenario 1, this section investigates the system's capability to absorb demand-side shocks. By incrementally increasing the demand surge ratio (0% to 35%), the study analyzes the transition from natural regulation to active intervention, and ultimately to physical collapse. Figs. 9 and 10 track the evolution of critical variables and compressor operating points throughout this process. In this analysis, gas sources are categorized based on their spatial proximity to user demand centers into remote resources, including the main source and the transfer source at Node 8, and proximal resources, including UGS, LNG, and the transfer source at Node 25. Fig. 10 illustrates the distribution of operating points of the CS-E compressor station, which is closest to the demand centers, on the compressor performance map under different demand surge ratios.

The background color zones in Fig. 9(a) clearly illustrate three representative operating regimes as the disturbance intensity increases. The boundaries between these regimes are strictly determined by the onset of load shedding and the system's resilience limit (i.e., the maximum disturbance maintaining the 4.0 MPa limit).

(1) Robust operating regime. The boundary of this regime represents the maximum disturbance the system can absorb purely through physical regulation without initiating load shedding. In this interval, the system absorbs shocks through the intrinsic flexibility of existing resources. Supply from both proximal and remote sources rises synchronously with demand. As shown in Fig. 10, compressor operating points shift

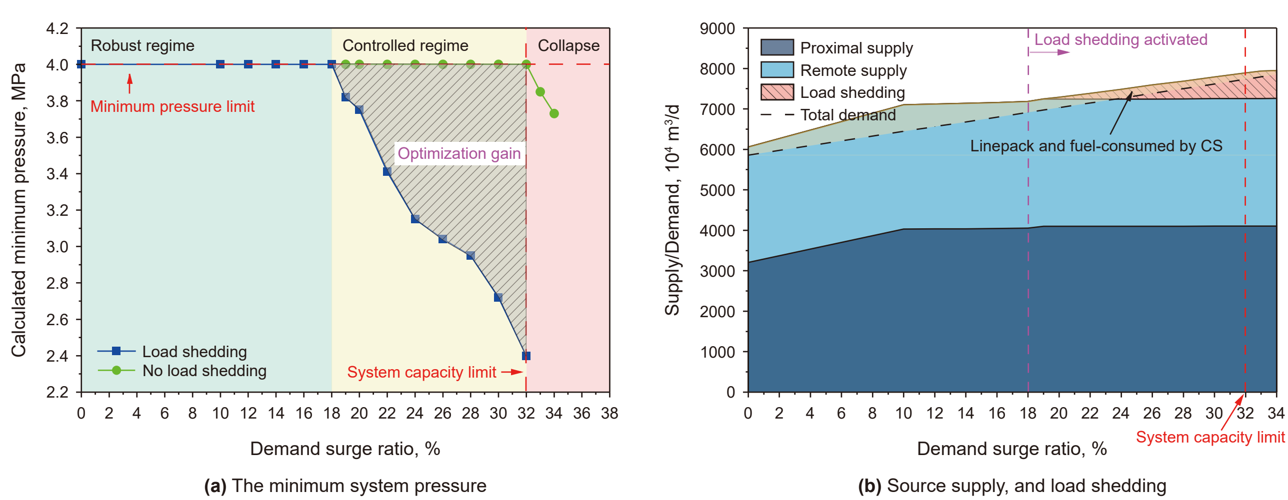

Fig. 9. The evolution of critical variables as the surge ratio varies.

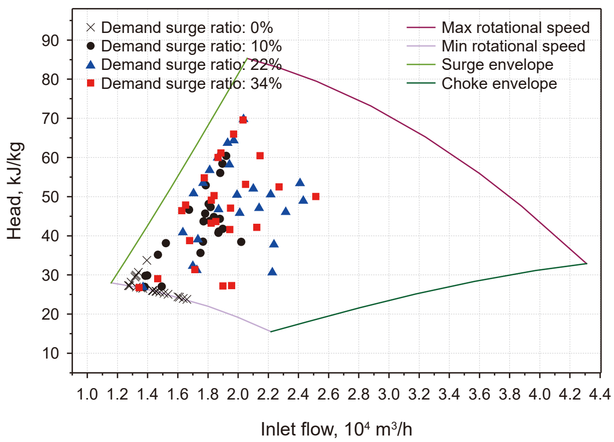

Fig. 10. The distribution of operating points of the CS-E compressor station.

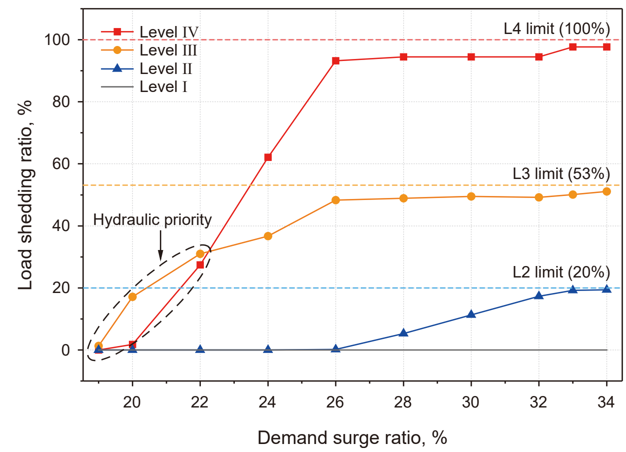

Fig. 11. The shedding ratios across different user priority levels.

from low-speed maintenance modes to high-efficiency regions, providing sufficient boosting to maintain nodal pressures above 4.0 MPa without external load shedding.

(2) Optimized control regime. This regime begins when load shedding becomes mandatory to prevent pressure violations. Its upper boundary defines the system's resilience limit, representing the maximum disturbance under which the system can still successfully maintain pressures above 4.0 MPa through optimized load shedding strategies. As the surge ratio exceeds 18%, the system status diverges significantly. Without optimization control, the minimum pressure rapidly breaches the safety threshold; conversely, under the load shedding strategy, the pressure is successfully maintained above critical levels, demonstrating clear optimization gains, as highlighted by the shaded region in Fig. 9(a). Appendix Table A.3 provides detailed resource allocation data for this stage, showing that the upstream gas source has reached its physical output limit while the downstream source still retains spare supply capacity. This spatial mismatch is corroborated by Fig. 10, where compressor operating points shift toward high-flow regions but remain in the middle of their pressure-ratio envelopes. This phenomenon confirms that the bottleneck has shifted from source availability to transmission efficiency. Due to the quadratic growth of frictional resistance, further boosting by compressors yields diminishing returns in downstream pressure recovery. Consequently, the model triggers load shedding. This measure reduces demand while improving the global pressure gradient, thereby partially restoring the effective transmission capability of remote sources, as evidenced by the secondary output growth of remote sources in Table A.3. Notably, the top of Fig. 9(b) shows that the sum of total supply and shedding slightly exceeds potential total demand. This is not an error but reflects the necessary linepack refilling process to restore pressure, alongside compressor self-consumption under limit states, highlighting that emergency operation must balance instantaneous supply-demand while compensating for previously overdrafted hydraulic potential.

(3) Physical collapse regime. This regime occurs when the disturbance exceeds the aforementioned resilience limit. As the surge ratio increases further to 32%, the system hits its physical capacity limit. Although load shedding approaches its maximum level, the optimized minimum pressure inevitably falls below 4.0 MPa. In this phase, compressor operating points in Fig. 10 become widely scattered. Some points show high flow but reduced head, indicating severe oscillations between attempted boosting and shedding-induced flow drops. This marks the complete exhaustion of transmission capacity. Failure at this stage is determined by inherent physical limits rather than scheduling strategy. The system simply cannot sustain higher demand shocks given the scale of fully protected high-priority loads.

Fig. 11 details the shedding ratios across different user priority levels as the surge ratio varies. Level I users remain unaffected throughout, validating the effectiveness of the hierarchical security mechanism under extreme conditions. When the demand surge ratio is below approximately 22%, the shedding ratio of Level III users exceeds that of the lower-priority Level IV users. Mirroring Scenario 1, this phenomenon is driven by spatial hydraulic effectiveness. Level III users are predominantly located at downstream terminal nodes where demand reduction offers high sensitivity for pressure restoration, whereas upstream Level IV shedding is attenuated by long-distance friction. However, as the surge exceeds 22%, the local bottleneck expands into a global system deficit. The optimization strategy then reverts to strict economic priority, drastically increasing the shedding of interruptible Level IV loads (>90%) to provide a hydraulic buffer for core users.

In summary, the demand surge analysis reveals that the system's resilience limit (identified at a 32% user demand surge) is fundamentally determined by topological transmission bottlenecks rather than the total availability of supply resources. Through the synergistic mechanism of linepack buffering, resource regulation, and priority-based shedding, the proposed optimization approach effectively extends the system's stable operation zone, ensuring the security of core livelihood gas supply until the physical infrastructure inevitably hits its absolute hydraulic limit.

5. Conclusions

This study develops a resilience-oriented optimization approach for emergency operation of natural gas pipeline systems from the perspective of transient operating mechanisms. The proposed approach integrates linepack dynamics, regulation capabilities of gas sources and compressor stations, and priority-based load shedding into a unified transient hydraulic formulation. In contrast to existing studies that primarily interpret resilience through probabilistic failure or statistical recovery metrics, resilience in this work is treated as an operational capability constrained by physical constraints. Its evolution under disturbances is fundamentally governed by the system's ability to maintain hydraulically feasible operating states.

Comparative analysis of supply-side interruptions and demand surges reveals that the dominant mechanisms of system resilience are highly dependent on the physical source of the disturbance:

(1) Under supply interruption scenarios, resilience is primarily shaped by the temporal coupling between passive linepack buffering and active scheduling timing. Linepack provides a finite but critical time window during which corrective actions remain effective. Specifically, utilizing this transient buffering capacity grants a 3–4 h survival window and avoids approximately 74.0% of unnecessary load shedding compared to traditional steady-state approaches. Delayed intervention nonlinearly amplifies subsequent load shedding requirements and risks compromising supply security for high-priority users. These findings indicate that resilience is sensitive to the decision window determined by linepack inertia.
(2) Conversely, in this study, resilience under demand surges is primarily constrained by topological transmission bottlenecks. As demand increases, system operation shifts from being supported by linepack and regulation flexibility to being bounded by inherent hydraulic capacity limits imposed by friction losses. In such specific scenarios, the resilience limit, which is identified at a 32% demand surge ratio, is dictated principally by the network topology and spatial hydraulic sensitivity, rather than total supply capacity. Although priority-based shedding extends the operational window, it cannot break through this physical ceiling.

The findings offer practical implications for emergency operation:

(1) Response timing: Excessive reliance on linepack buffering is a double-edged sword; timely intervention within the survival time is crucial to avoid escalating hydraulic costs.
(2) Physical limits: Near physical operating limits, further strengthening supply-side regulation or compressor operation yields diminishing returns due to transmission congestion.
(3) Shedding strategy: Under specific topological constraints, effective load shedding should balance simple economic prioritization with spatial hydraulic effectiveness (i.e., prioritizing loads that are hydraulically sensitive to critical low-pressure nodes when transmission bottlenecks dominate).

Finally, it should be noted that the proposed approach, based on a fixed compressor unit commitment, is primarily applicable to short-term transient emergencies. For prolonged disturbances with continuously increasing demand, the evaluated resilience limits serve as a conservative baseline. Future research will focus on extending this approach to address discrete commitment decisions (e.g., compressor start-up sequences) and incorporating uncertainties from renewable energy injection, ultimately broadening the scope to integrated energy system resilience.

CRediT authorship contribution statement

Si-Rui Zhao: Writing – original draft, Visualization, Validation, Software, Methodology, Formal analysis, Conceptualization. **Li-Li Zuo:** Writing – review & editing, Validation, Supervision, Methodology, Formal analysis, Conceptualization. **Feng Zhu:** Writing – review & editing, Validation, Supervision, Resources. **Bing-Lang He:** Validation, Data curation. **Chang-Chun Wu:** Writing – review & editing, Validation, Supervision, Formal analysis, Conceptualization.

Declaration of competing interest

The authors declare that they have no known competing financial interests or personal relationships that could have appeared to influence the work reported in this paper.

Acknowledgment

The work is supported by the Oil & Gas Major Project (2025ZD14016000).

Appendix

Table A.1
Specific parameters of users in the case study.

User ID	User type	Node ID	Priority level	Max load shedding coefficient
1	City gas	5	I	0
2	City gas	6	I	0
3	Power plant	6	IV	1
4	Industrial	6	III	0.5
5	City gas	8	I	0
6	CNG	8	I	0
7	City gas	9	I	0
8	City gas	11	I	0
9	City gas	12	I	0
10	City gas	13	I	0
11	City gas	15	I	0
12	Chemical	15	III	0.4
13	City gas	16	I	0
14	Chemical	16	I	0
15	City gas	17	I	0
16	City gas	17	II	0.2
17	CNG	17	I	0
18	Chemical	17	III	0.4
19	Power plant	17	IV	1
20	CNG	18	I	0

Table A.1 (*continued*)

User ID	User type	Node ID	Priority level	Max load shedding coefficient
21	City gas	18	I	0
22	Power plant	18	I	0
23	City gas	19	I	0
24	City gas	20	I	0
25	Power plant	20	IV	1
26	City gas	21	II	0.2
27	City gas	21	I	0
28	City gas	22	II	0.2
29	Power plant	23	IV	1
30	City gas	23	I	0
31	CNG	23	I	0
32	City gas	24	I	0
33	City gas	25	I	0
34	City gas	25	II	0.2
35	CNG	25	I	0
36	Power plant	25	III	0.6
37	CNG	26	I	0
38	Industrial	26	III	0.5
39	City gas	26	I	0

Table A.2
Sensitivity analysis of system survival time under different time steps in Scenario 1.

Time step	System survival time	Minimum nodal pressure, MPa	Total shedding volume, m^3	Computation time, s
1 h	3–4 h	3.980	79.68×10^4	23.6
30 min	3–3.5 h	3.983	77.69×10^4	49.1
15 min	3.25–3.5 h	3.992	76.34×10^4	113.7

Table A.3
Variations in resource supply and load shedding with respect to surge ratios.

Demand surge ratio	Proximal supply, 10^4 m^3/d	Remote supply, 10^4 m^3/d	Load shedding, 10^4 m^3/d
10%	4030	3071	0
12%	4033	3084	0
14%	4037	3097	0
16%	4042	3112	0
18%	4052	3131	0
19%	4100	3142	3.22
20%	4097	3142	47.57
22%	4098	3142	142.13
24%	4097	3144	239.08
26%	4097	3144	349.63
28%	4097	3149	435.72
30%	4100	3149	534.08
32%	4100	3150	632.80
33%	4100	3150	681.15
34%	4100	3153	689.55

References

Ameli, H., Qadrdan, M., Strbac, G., 2017. Value of gas network infrastructure flexibility in supporting cost effective operation of power systems. Appl. Energy 202, 571–580. https://doi.org/10.1016/j.apenergy.2017.05.132.

Asadzadeh, S.M., Maleki, H., Tanhaeean, M., 2020. A resilience engineering-based approach to improving service reliability in maintenance organizations. Int. J. Syst. Assur. Eng. Manag. 11 (5), 909–922. https://doi.org/10.1007/s13198-020-01015-5.

Chen, Q., Wu, C., Zuo, L., et al., 2021. Multi-objective transient peak shaving optimization of a gas pipeline system under demand uncertainty. Comput. Chem. Eng. 147, 107260. https://doi.org/10.1016/j.compchemeng.2021.107260.

Ghilardi, L.M.P., Naik, S., Martelli, E., et al., 2025. Economic nonlinear model predictive control for cyclic gas pipeline operation. Comput. Chem. Eng. 196, 109039. https://doi.org/10.1016/j.compchemeng.2025.109039.

Huang, W., Li, Y., Yu, W., et al., 2021. An evaluation index system of the user satisfaction for the natural gas pipeline network. J. Pipeline Sci. Eng. 1 (4), 452–458. https://doi.org/10.1016/j.jpse.2021.11.001.

Jia, Q., Li, Y., Hu, Q., et al., 2025. Analysis of the dynamic behavior of supercritical CO_2 pipeline based on the nonisothermal transient flow model. Energy Fuels 39 (11), 5463–5478. https://doi.org/10.1021/acs.energyfuels.4c06010.

Koo, B., 2022. Comparison of finite-volume method and method of characteristics for simulating transient flow in natural-gas pipeline. J. Nat. Gas Sci. Eng. 98, 104374. https://doi.org/10.1016/j.jngse.2021.104374.

LeVeque, R.J., 1992. In: Numerical Methods for Conservation Laws, second ed. Birkhäuser, Basel. https://doi.org/10.1007/978-3-0348-8629-1.

Li, B., Chen, Y., Wei, W., et al., 2022. Online coordination of LNG tube trailer dispatch and resilience restoration of integrated power-gas distribution systems. IEEE Trans. Smart Grid 13 (3), 1938–1951. https://doi.org/10.1109/TSG.2022.3141548.

Liu, E.-B., Peng, Y., Peng, S.-B., et al., 2022. Research on low carbon emission optimization operation technology of natural gas pipeline under multi-energy structure. Pet. Sci. 19 (6), 3046–3058. https://doi.org/10.1016/j.petsci.2022.09.025.

Liu, M., Yuan, Y., Xu, A., et al., 2025. A learning-based artificial bee colony algorithm for operation optimization in gas pipelines. Inf. Sci. 690, 121593. https://doi.org/10.1016/j.ins.2024.121593.

Malik, S.N., Sukhera, O.R., 2012. Management of natural gas resources and search for alternative renewable energy resources: a case study of Pakistan. Renew. Sustain. Energy Rev. 16 (2), 1282–1290. https://doi.org/10.1016/j.rser.2011.10.003.

Marino, A., Zio, E., 2021. A framework for the resilience analysis of complex natural gas pipeline networks from a cyber-physical system perspective. Comput. Ind. Eng. 162, 107727. https://doi.org/10.1016/j.cie.2021.107727.

Meng, Y., Chen, R., Deng, T., 2022. Two-stage robust optimization of power cost minimization problem in gunbarrel natural gas networks by approximate dynamic programming. Pet. Sci. 19 (5), 2497–2517. https://doi.org/10.1016/j.petsci.2021.09.048.

Patriarca, R., Bergström, J., Di Gravio, G., et al., 2018. Resilience engineering: current status of the research and future challenges. Saf. Sci. 102, 79–100. https://doi.org/10.1016/j.ssci.2017.10.005.

Qian, L., Bai, Y., Wang, W., et al., 2023. Natural gas crisis, system resilience and emergency responses: a China case. Energy 276, 127500. https://doi.org/10.1016/j.energy.2023.127500.

Qin, C., Wang, Y., Ye, S., 2025. Two-stage resilience enhancement method for integrated electricity-gas systems through linepack and mobile compressors. Int. J. Electr. Power Energy Syst. 168, 110722. https://doi.org/10.1016/j.ijepes.2025.110722.

Raheli, E., Werner, Y., Kazempour, J., 2025. Flexibility of integrated power and gas systems: Gas flow modeling and solution choices matter. IEEE Trans. Power Syst. 40 (3), 2130–2142. https://doi.org/10.1109/TPWRS.2024.3502541.

Schill, R., Costescu, A., Gandossi, L., et al., 2025. Resilience indicators for the EU natural gas system. Environ. Syst. Decis. 45 (4), 61. https://doi.org/10.1007/s10669-025-10052-z.

Senderov, S.M., Vorobev, S.V., Smirnova, E.M., 2022. Peak underground gas storage efficiency in reducing the vulnerability of gas supply to consumers in an extensive gas transmission system. Reliab. Eng. Syst. Saf. 221, 108352. https://doi.org/10.1016/j.ress.2022.108352.

Sesini, M., Giarola, S., Hawkes, A.D., 2022. Solidarity measures: assessment of strategic gas storage on EU regional risk groups natural gas supply resilience. Appl. Energy 308, 118356. https://doi.org/10.1016/j.apenergy.2021.118356.

Shan, X., Yu, W., Gong, J., et al., 2023. A methodology to evaluate gas supply reliability of natural gas pipeline network considering the effects of natural gas resources. Reliab. Eng. Syst. Saf. 238, 109431. https://doi.org/10.1016/j.ress.2023.109431.

Su, H., Zio, E., Zhang, Z.-J., et al., 2022. Development of an integrated dynamic model for supply security and resilience analysis of natural gas pipeline network systems. Pet. Sci. 19 (2), 761–773. https://doi.org/10.1016/j.petsci.2021.10.002.

Tasseff, B., Coffrin, C., Bent, R., et al., 2022. Natural gas maximal load delivery for multi-contingency analysis. Comput. Chem. Eng. 168, 108032. https://doi.org/10.1016/j.compchemeng.2022.108032.

Wächter, A., Biegler, L.T., 2006. On the implementation of an interior-point filter line-search algorithm for large-scale nonlinear programming. Math. Program. 106 (1), 25–57. https://doi.org/10.1007/s10107-004-0559-y.

Wang, C., Zhou, D., Xiao, W., et al., 2023. Research on the dynamic characteristics of natural gas pipeline network with hydrogen injection considering line-pack influence. Int. J. Hydrogen Energy 48 (65), 25469–25486. https://doi.org/10.1016/j.ijhydene.2023.03.298.

Wen, K., Jiao, J., Zhao, K., et al., 2023. Rapid transient operation control method of natural gas pipeline networks based on user demand prediction. Energy 264, 126093. https://doi.org/10.1016/j.energy.2022.126093.

Yang, X., Chen, K., Liu, M., et al., 2025. Research on the connectivity reliability analysis and optimization of natural gas pipeline network based on topology. Sci. Rep. 15 (1), 13442. https://doi.org/10.1038/s41598-025-98749-8.

Yang, Z., Su, H., Du, X., et al., 2023. Supply resilience assessment of natural gas pipeline network systems. J. Clean. Prod. 385, 135654. https://doi.org/10.1016/j.jclepro.2022.135654.

Ye, H., Li, Z., Li, G., et al., 2022. Topology analysis of natural gas pipeline networks based on complex network theory. Energies 15 (11), 3864. https://doi.org/10.3390/en15113864.

Yu, D., Ning, X., Xiang, Q., et al., 2024. Optimization method of natural gas pipeline network emergency dispatch based on particle swarm optimization. In: Computational and Experimental Simulations in Engineering, pp. 481–491. https://doi.org/10.1007/978-3-031-44947-5_38.

Zhao, S., Zuo, L., Cao, Y., et al., 2026. An ANN-embedded MILP approach for optimizing the steady-state operation of gas pipeline networks. Chem. Eng. Sci. 320, 122619. https://doi.org/10.1016/j.ces.2025.122619.

Zhao, Z., Yang, Z., Su, H., et al., 2025. A methodology of natural gas pipeline network system supply resilience optimization: based on demand-side and data science-driven approach. Reliab. Eng. Syst. Saf. 261, 111071. https://doi.org/10.1016/j.ress.2025.111071.

Zhou, D., Jia, X., Ma, S., et al., 2022. Dynamic simulation of natural gas pipeline network based on interpretable machine learning model. Energy 253, 124068. https://doi.org/10.1016/j.energy.2022.124068.